EXPERIMENTAL COMPARISON OF A SINGLE SCREW EXPANDER UNDER DIFFERENT OPERATING CONDITIONS AND WORKING FLUIDS

Sergei Gusev*, Davide Ziviani, Martijn van den Broek

Department of Flow, Heat and Combustion Mechanics, Ghent University,
Ghent, Belgium
servei.gusev@ugent.be, davide.ziviani@ugent.be, martijn.vandenbroek@ugent.be

* Corresponding Author

ABSTRACT

During the last years, one of the most popular ways to recover low-grade waste heat is the organic Rankine cycle (ORC). This technology is widely studied and continuously optimized and, as a result, there are many efficient installations available on the market utilizing heat with stable parameters such as from geothermal sources or from the biomass combustion process. However, if a variable hot source in terms of either temperature or flow rate is introduced, the expansion devices have to work at non-optimal conditions, which decrease the global efficiency of ORC installations, e.g. in the case of waste heat recovery. In order to characterize the performance of a positive displacement expander close enough to the optimum, the influence of pressure ratios, filling factor, and working fluid properties on power output is studied. In this paper, experimental results obtained on a small-scale ORC test setup based on an 11 kWe single-screw expander are presented. Two working fluids are used during the tests, i.e. R245fa and SES36 (Solkatherm). These working fluids are common for ORC installations exploiting low-temperature waste heat. The waste heat source is simulated by an electrically heated thermal oil loop with adjustable temperature and flow rate. Various waste heat inlet flow rates are considered in order to find an optimal evaporation pressure and to maximize the power output with different heat source profiles. Based on the experimental data, the expander model is developed. For each working fluid, optimal working conditions are determined. In most cases, there is under-expansion due to a relatively small built-in volume ratio, causing certain losses. By means of the model, the ideal expansion process is simulated and compared with the real one obtained experimentally to quantify these losses and conclusions can be drawn whether significant benefits can be offered by using an optimized expander instead of an ”off-the-shelf” reversed compressor.

1. INTRODUCTION

The organic Rankine cycle (ORC) is mainly used to produce electricity or useful work from heat at lower temperature, which are renewable energy sources, such as solar or geothermal, and low-grade heat produced in an industrial process which cannot be recovered (van den Broek et al., 2012). Solar, with exception of concentrated solar technologies, and geothermal applications are often also characterized by relatively low temperature levels. The ORC technology utilizes this heat, reducing the use of primary energy and CO_2 emission.

A test rig (Fig. 1) was built to demonstrate the ORC technology in the frame of a project granted by IWT Flanders and it is currently used in the ORCNext project (www.orcnext.be) aiming to improve the ORC technology by introducing new types of expanders, advanced cycles, model based predictive control algorithms in combination with an economical analysis. The results obtained during extensive experiments are introduced in this paper in order to contribute to the study on the working fluids behavior in actual installations, e.g. Bracco et al. (2013) and Farrokhi et al. (2013), and to evaluate the impact of different working fluids on the same installation (Huck et al., 2013). While theoretical investigations on

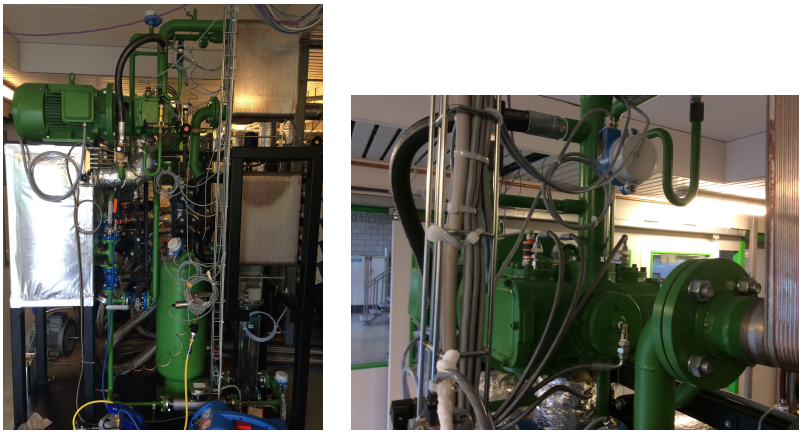

(a) (b)

Figure 1: (a) ORC at UGent, Campus Kortrijk; (b) close view of the single screw expander installed.

the comparison of fluid properties can be found in literature e.g. Badr et al. (1985); Saleh et al. (2007); Quoilin et al. (2011), publications about practical use of different fluids and the relative performance are still rare. In this work, the performance of a unit built from "off the shelf" components and filled subsequently with two working fluids SES36 (Solkatherm) and R245fa is mapped and analyzed, the maximum power output regimes are indicated.

2. ORC TEST SETUP

The ORC test setup is shown in Fig. 1(a). A standard single-screw air compressor has been adjusted by BEP Europe (Ziviani et al., 2014) to operate as an expansion device and connected to an asynchronous generator with 11 kWe nominal electric power. A closer view of the expander is shown in Fig. 1(b). The electrical power produced by the generator is injected into the electric grid by means of a four-quadrant inverter, which also allows to vary the generator rotational speed from 0 to 3600 rpm. The speed of a circulating 14-stage centrifugal pump can also be varied from 0 to 3000 rpm introducing a variable evaporation pressure up to 14 bar. The evaporator, internal heat exchanger and the condenser are three identical brazed plate heat exchangers. A more detailed description of the setup and the sensors installed can be found in a previous publication (Gusev et al., 2014). Thermodynamic parameters which can not be measured directly are calculated in real time using the CoolProp library (Bell et al., 2014). In this analysis, the power consumed by auxiliary equipment is neglected. The thermal power input, $\dot{Q}_{T66,ev,in}$, is guaranteed by a controllable 250 kW electric heater with Therminol 66 (T66) as working medium. The electric power injected to the grid is measured by the inverter. The net power produced by the ORC is obtained by subtracting the pump power from the electric power measured at the grid:

$$\dot{W}_{el,net} = \dot{W}_{el,grid,exp} - \dot{W}_{pp} \tag{1}$$

Due to the absence of a torque meter to measure the expander shaft power, an overall isentropic efficiency that includes the expander and the generator/inverter is defined as follows:

$$\eta_{is,oa,meas} = \frac{\dot{W}_{el,grid,exp}}{\dot{W}_{is,exp}} = \frac{\dot{W}_{el,grid,exp}}{\dot{m}_{r,exp}\left(h_{su,exp} - h_{ex,is,exp}\right)} \tag{2}$$

In order to obtain the isentropic efficiency at the shaft, the generator efficiency and the inverter effectiveness should be accounted for as follows,

$$\eta_{is,sh,exp} = \frac{\dot{W}_{sh,exp}}{\dot{W}_{is,exp}} = \frac{\dot{W}_{el,grid,exp}}{\eta_{mech,gen}\,\epsilon_{el,inv}\left[\dot{m}_{r,exp}\left(h_{su,exp} - h_{ex,is,exp}\right)\right]} \tag{3}$$

The correlations for the generator and the inverter efficiency have been obtained from Melotte (2012). The filling factor is given by:

$$\Phi_{FF} = \frac{\dot{m}v_{su,exp}}{\dot{V}_{swept,th}} = \frac{\dot{m}v_{su,exp}}{2\,z_{sr}\,V_{g,su}\,\left(N_{rot,exp}/60\right)} \tag{4}$$

where the volume of the groove at suction closure, $V_{g,su}$, is determined by the geometric model described in details in Ziviani et al. (2015). Finally, the net cycle efficiency can be expressed as:

$$\eta_{ORC,net} = \frac{\dot{W}_{el,grid,exp} - \dot{W}_{pp}}{\dot{Q}_{T66,ev,in}} \tag{5}$$

The main measured and calculated parameters for both working fluids are summarized in Table 1.

3. EXPERIMENTAL RESULTS

The choice of the experiment operating conditions is based on some typical solar and geothermal applications described in literature (Barbier, 2002; Tchanche et al., 2009; Liu et al., 2013; Zhou, 2014). The temperature of the heat source in many cases is stable over time and therefore has been kept constant during the experiments. Typical temperature range of the heat source considered is between 90 °C and 125 °C. However, the maximum temperature of the heat carrier (Therminol66) is limited to 125 °C because of the expander design that does not allow higher operating temperatures. Another limitation is represented by the maximum pressure that the expander can handle safely. Throughout the tests, the maximum pressure never exceeded 14 bar. The operating conditions of the working fluids are shown in Fig. 2. It can be noted that the condensing pressure of SES36 is typically below atmospheric pressure. Challenges arise to avoid air infiltration in the system, in particular during the idle state. In fact, the design of the installation does not allow to completely prevent leakages because the components are designed for general purposes.

The first experiments were performed with SES36 and successively the installation has been charged with R245fa. Due to the fact that the installation relies on an air-cooler installed on the roof top, the cooling capacity strongly depends on the weather conditions. The fluids have been tested in different months of the year and therefore it is not possible to draw general conclusions on the maximum performance achievable by the system. However, a comparison of the operating conditions of the ORC with the different working fluid has been carried out. Two typical thermodynamic plots (T-s diagram) of the cycle with SES36 and R245fa are shown in Fig. 3.

In order to maintain a stable operation of the setup, a certain superheating level of 10-15 K before the expander was kept, in the case of SES36. The maximum achievable evaporating pressure in this case was about 8 bar, therefore the same pressure was used during the R245fa experiments in order to have a fair comparison. The superheating level of R245fa at the same conditions is much higher, up to 40 K. This cycle configuration leads to a significant exergy loss. Potentially, the heat source can be cooled down much deeper if a lower flow rate is chosen. As a result, a lower power output is detected. Moreover, during the experiments with SES36, a significant subcooling was detected.

One of the aims of the experimental campaign was the characterization of the expander with two different fluids and under different operating conditions. To this end, the mass flow rate is imposed by adjusting the frequency of the pump. However, it was noted that also the rotational speed of the expander influences the mass flow rate of the system. One of the reasons is that the pump is a centrifugal-type and as a consequence the mass flow rate is dependent on the evaporation pressure. Instead the expander is a volumetric machine and the volumetric flow rate is only dependent on the rotational speed. The tests were conducted by varying the frequency of the pump from minimum to maximum at a fixed expander rotational speed. The same procedure has been applied for all the considered expander rotational speeds. In particular, for SES36 only 2000 rpm and 3000 rpm have been tested. Four different speeds have been

Table 1: Summary of the minimum and maximum measured values of the variables considered for both working fluids.

	$p_{su,exp}$ (kPa)	$p_{ex,exp}$ (kPa)	$T_{su,exp}$ (°C)	$\dot{m}_r$ (kg/s)	$\dot{W}_{el,grid}$ (W)	$T_{ex,exp}$ (°C)	T_{cd} (°C)	ΔT_{sh} (K)	ΔT_{sc} (K)	$\eta_{is,oa,exp}$ (-)	η_{ORC} (-)	Φ_{FF} (-)
SES36												
Min	450	90.6	91.65	0.150	1283	73.99	30.91	0.13	9	0.135	0.010	0.897
Max	1028	177.9	125	0.406	7865	102.0	50.87	28	14	0.647	0.092	1.117
R245fa												
Min	566	120	106.7	0.12	1283	75.5	18.82	26	1.9	0.205	0.014	1.038
Max	1230	232	124.9	0.37	7364	104.6	37.12	56	3.7	0.519	0.077	1.331

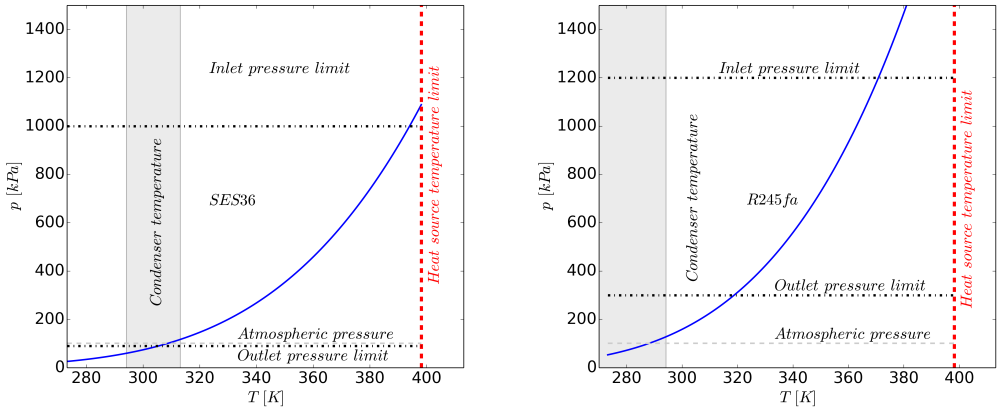

(a) (b)

Figure 2: Working fluid operating conditions during the tests: (a) SES36; (b) R245FA.

tested in the case of R245fa, i.e. 2000 rpm, 2500 rpm, 3000 rpm and 3300 rpm. A total of 43 and 59 steady-state points have been determined for SES36 and R245fa, respectively. The comparison of the fluids is proposed in terms of operating maps as function of power output, isentropic efficiency, mass flow rate, pump and expander rotational speeds as well as ORC efficiency.

4. COMPARISON OF THE WORKING FLUIDS PERFORMANCE

As it can be seen in Fig. 2, an ORC unit filled with R245fa operates at higher working pressures compared with SES36, resulting in lower pressure ratios within the same temperature region. As a consequence, the thermodynamic efficiency of the ORC running with R245fa is slightly lower. The condenser pressure is very close to the expander limit of 3 bar, especially during summer. This pressure corresponds to a temperature of about 45 °C. Taking into account a certain temperature difference between the condenser and the ambient temperatures caused by the air-type cooling loop, the current combination of working fluid and expander is not appropriate for regions with a hot climate. An expander suitable to withstand higher working pressures is needed in order to avoid emergency shut-downs if R245fa is used. An advantage of R245fa over SES36 is that the condensing pressure is higher than the ambient which prevents non-condensable gases in the system. On the other hand, higher working pressures mean in general higher leakage flows and the loss of working fluid through flanges and shaft seals. The cost of the low-GWP working fluids is non-negligible especially for larger installations. The absence of subcooling caused by non-condensable gasses in the condenser is an advantage from a thermodynamic point of view but increases the duty of the circulating pump. A saturated working fluid can start boiling in the suction line due to a certain local pressure drop preventing pump to work properly. In some cases under a variable

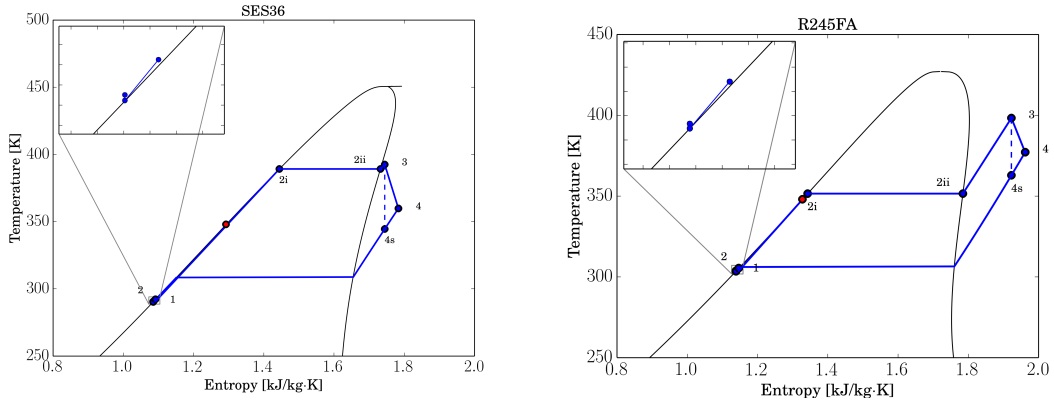

(a) (b)

Figure 3: Examples of thermodynamic plots obtained from the experiments:(a) SES36 ;(b) R245fa. The outlet state of the regenerator prior entering the evaporator is marked with a red dot.

cooling temperature this phenomenon can completely block the flow.

The steady-state points obtained for both fluids are plotted in Fig. 4, where the power output of the expander, $\dot{W}_{el,grid}$, is given as function of the pressure ratio, $r_{p,exp}$, for different rotational speeds. The isentropic efficiency is indicated by a color scale. It is possible to notice that there is a quasi-linear trend between power output and pressure ratio.

For most of the points, the power output increases with the increase of both pressure ratio and rotational speed. This can be easily observed by considering the rotational speeds of 2000 rpm and 3000 rpm. Regarding the rotational speeds of 2500 rpm and 3300 rpm for R245fa, shown in Fig. 4(b), a similar consideration can be made, i.e. the higher the rotational speed and the pressure ratio, the higher the power output, by keeping in mind that these steady-state points were obtained during a very warm day which affected the condensing pressure. The pressure ratio range achievable was limited both at high pressure side (limit set by maximum pressure of expander) and low pressure side because of high external temperature.

The ORC installation operates most of the time at pressure ratios higher than the pressure ratio corresponding to the built-in volume ratio of the expander, $r_{v,built-in}$ = 4.7 (Ziviani et al., 2015), causing an over-expansion. While the power output at the same pressure ratio is similar for both fluids, the expander isentropic efficiency is slightly higher in the case of SES36. At low pressure ratios and power, the influence of the expander rotational speed is limited. Maximum and minimum values of the performance of each fluid are listed in Table 1.

The operating conditions of both working fluids are presented with three performance maps shown in Fig. 5, 6, 8. In Fig. 5, 6, the mass flow rates of SES36 and R245fa and the isentropic efficiency versus the expander and the pump rotational speeds are shown , respectively. A higher mass flow of R245fa at the same conditions is caused by its lower density in comparison with SES36. The influence of the expander rotational speed is less significant than the pump rotational speed for both fluids. The trend for the pump rotational speed is almost linear, as shown in Fig. 7, so higher rotational speeds can be recommended in order to achieve a higher performance. The maximum isentropic efficiency of the expander is achieved at the nominal speed of 3000 rpm for both fluids. The third set of performance maps, in Fig. 8, assesses the optimum operating conditions, in terms of cycle efficiency, η_{ORC}, of the ORC system for different thermal input, $\dot{Q}_{T66}$, and degree of superheating, ΔT_{sh}. The cycle efficiency is related to the degree of superheating and the working fluid. In particular, in the case of SES36, the maximum cycle efficiency is observed with a range of the degree of superheating of 5-10 K, as shown in Fig. 8(a). Instead, in the

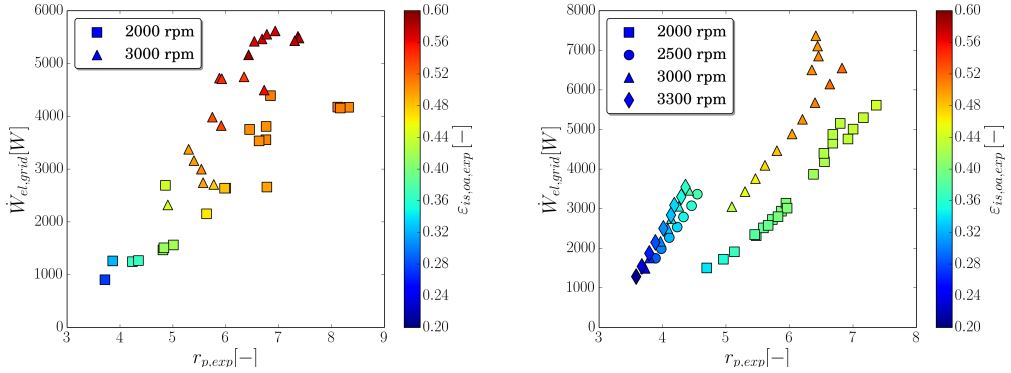

(a) (b)

Figure 4: Power output as a function of different pressure ratios: (a) SES36 ;(b) R245fa. The color scale indicates the overall isentropic efficiency.

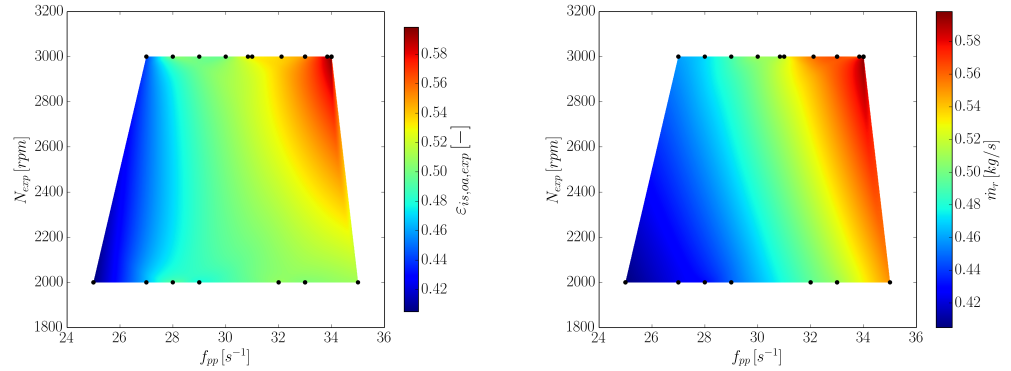

(a) (b)

Figure 5: Operating maps of SES36: (a) overall isentropic efficiency as function of pump and expander rotational speeds; (b) mass flow rate as function of pump and expander rotational speeds.

case of R245fa, the cycle efficiency is maximized at higher values of the superheating, 30-35 K, Fig. 8(b).

The operating stability of the system and different conditions have also been investigated. During the experiments, an unstable operation characterized by a fluctuating mass flow rate of the working fluid was detected when the working fluid was entering the expander close to the vapor saturation point. A decrease of the evaporation pressure resulted in an increase of the mass flow rate, which is a sign of a wet expansion. A drop in both power output and isentropic efficiency occurred.

5. CONCLUSIONS

In this paper, the performance of an non-optimized ORC unit operating subsequently with two different working fluids under the same conditions is mapped. The efficiency of the ORC system components is not constant during operation and it is influenced by the dynamic behavior of each component. Based on the experimental results, an optimal rotational speed of the circulating pump and the expander can be found for each typical working condition such as the flow rate, the temperature of the heat source and the ambient temperature. These settings could be implemented in a feed-forward control of an installation the operates with a variable heat input.

For the given temperature level and the current installation, SES36 is more optimal than R245fa. For

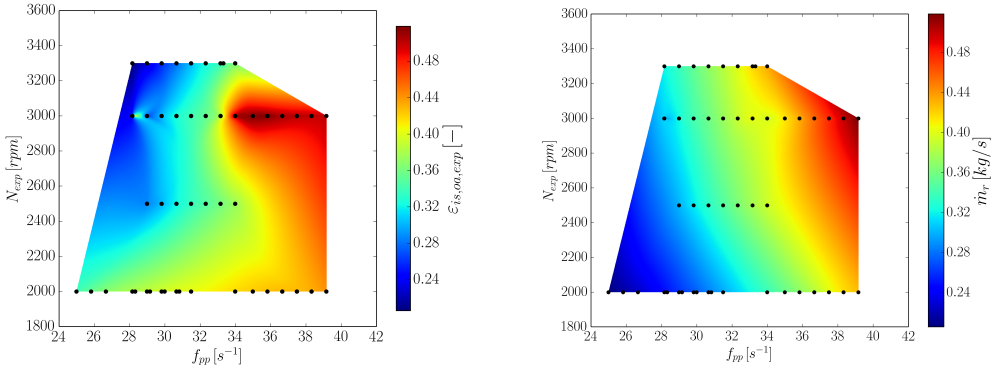

(a) (b)

Figure 6: Operating maps of R245fa: (a) overall isentropic efficiency as function of pump and expander rotational speeds; (b) mass flow rate as function of pump and expander rotational speeds.

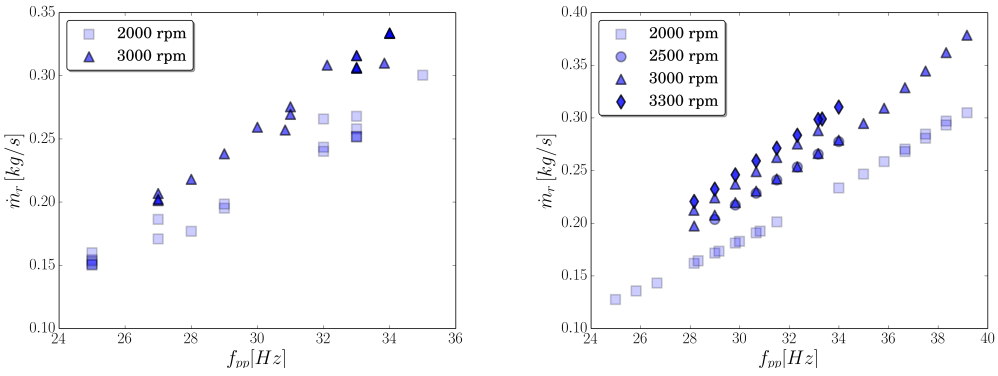

(a) (b)

Figure 7: Influence of the pump frequency on the mass flow rate at different expander rotational speeds: (a) SES36; (b) R245fa.

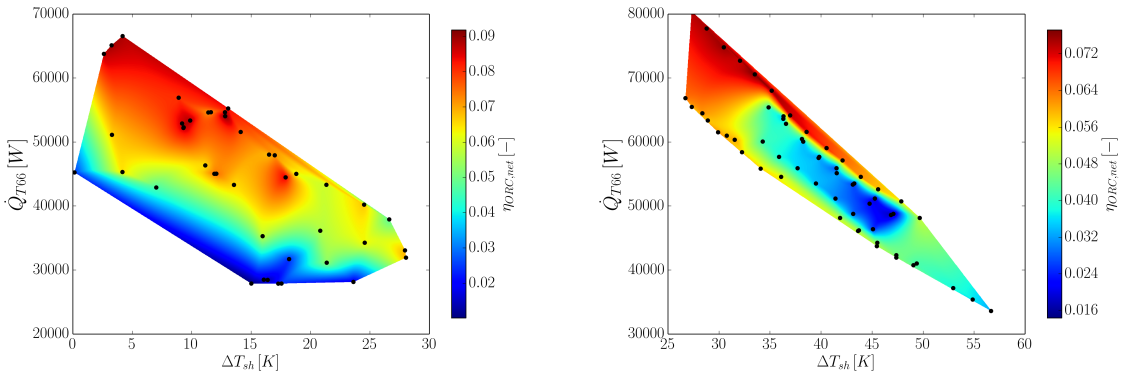

(a) (b)

Figure 8: Net cycle efficiency as function of thermal power and degree of superheating: (a)SES36; (b) R245FA.

both fluids, operation at superheating levels lower than 5 K should be avoided due to difficulties in maintaining a stable mass flow rate.

REFERENCES

Badr, O., Probert, S. D., and O'Callaghan, P. (1985). Selecting a working fluid for a Rankine cycle engine. *Applied Energy*, 21:1–42.

Barbier, E. (2002). Geothermal energy technology and current status: an overview. *Renewable and Sustainable Energy Reviews*, 6:3–65.

Bell, I. H., Wronski, J., Quoilin, S., and Lemort, V. (2014). Pure and pseudo-pure fluid thermophysical property evaluation and the open-source thermophysical property library CoolProp. *Industrial & Engineering Chemistry Research*, 53(6):2498–2508.

Bracco, R., Clemente, S., Micheli, D., and Reini, M. (2013). Experimental tests and modelization of a domestic-scale ORC (organic Rankine cycle). *Energy*, 58(1):107–116. ISSN 0360-5442.

Farrokhi, M., Noie, S. H., and Akbarzadeh, A. A. (2013). Preliminary experimental investigation of a natural gas-fired ORC-based micro-CHP system for residential buildings. *Applied Thermal Engineering*, 7. ISSN 1359-4311.

Gusev, S., Ziviani, D., Bell, I., De Paepe, M., and van den Broek, M. (2014). Experimental comparison of working fluids for organic Rankine cycle with single-screw expander. In *Proceedings of the International Refrigeration and Air Conditioning Conference*. Paper 1548.

Huck, P., Laursen, A. L., Zia, J., and Woolley, L. (2013). Identification and test of low global warming potential alternatives to HFC-245fa in organic Rankine cycles. In *Proceedings of the 2nd International Seminar on ORC Power Systems*, Rotterdam, Netherlands.

Liu, Q., Duan, Y., and Yang, Z. (2013). Performance analyses of geothermal organic Rankine cycles with selected hydrocarbon working fluids. *Energy*, 63:123–132. ISSN 0360-5442.

Melotte, N. (2012). Experimental study and dynamic modeling of a waste heat recovery organic Rankine cycle. Master's thesis, University of Liege.

Quoilin, S., Declaye, S., Tchanche, B. F., and Lemort, V. (2011). Thermo-economic optimization of waste heat recovery organic Rankine cycles. *Applied Thermal Engineering*, 31(14):2885–2893.

Saleh, B., Koglbauer, G., Wendland, M., and Fischer, J. (2007). Working fluids for low temperature organic Rankine cycles. *Energy*, 32:1210–1221.

Tchanche, B. F., Papadakis, G., Lambrinos, G., and Frangoudakis, A. (2009). Fluid selection for a low-temperature solar organic Rankine cycle. *Applied Thermal Engineering*, 29:2468–2476.

van den Broek, M., Vanslambrouck, B., and De Paepe, M. (2012). Electricity generation from biomass: Organic Rankine cycle versus steam cycle. In *Proceedings of the Conference and Exhibition on Biomass for Energy*, Jönköping, Sweden.

Zhou, C. (2014). Hybridisation of solar and geothermal energy in both subcritical and supercritical organic Rankine cycles. *Energy Conversion and Management*, 81:72–82. ISSN 0196-8904.

Ziviani, D., Bell, I., van den Broek, M., and De Paepe, M. (2014). Comprehensive model of a single-screw expander for ORC-systems. In *Proceedings of the International Compressor Engineering Conference*. Paper 2357.

Ziviani, D., Bell, I. H., De Paepe, M., and van den Broek, M. (2015). Update on single-screw expander geometry model integrated into an open-source simulation tool. In *9th Int. Conf. on Compressors and their Systems, City University of London, London*, number 39.

NOMENCLATURE

c_p	specific heat at constant pressure	(J/kg-K)	**Subscript**	
$\dot{m}$	mass flow rate	(kg/s)	exp	expander
f_{pp}	pump frequency	(Hz)	el	electric
N	rotational speed	(rpm)	ev	evaporator
p	pressure	(Pa)	gen	generator
$\dot{Q}$	heat rate	(W)	is	isentropic
r_p	pressure ratio	(-)	in	inlet
T	temperature	(K, °C)	inv	inverter
v	specific volume	(m^3/kg)	meas	measured
V	volume	(m^3)	oa	overall
$\dot{W}$	power	(W)	pp	pump
z_{sr}	number of starwheel tooth	(-)	r	refrigerant
Φ_{FF}	filling factor	(-)	sc	subcooling
ϵ	effectiveness	(-)	su	supply
η	efficiency	(-)	sh	superheating
Subscript				shaft
cd	condenser		th	theoretical
ex	exhaust		T66	Therminol66

ACKNOWLEDGEMENT

The financial support is provided by the Institute for the Promotion and Innovation by Science and Technology in Flanders. All data and results presented in this survey have been obtained in the frame of the IWT SBO-110006 project “The Next Generation Organic Rankine Cycles”: www.orcnext.be